Thermal localization and rheological control on the steady-state width of 1D ductile shear zones

N.M. Beeler USGS science for a changing world Hannah Shabtian, Greg Hirth BROWN

Acknowledgements: This study was supported by the USGS Earthquake Hazards Program and the Statewide California Earthquake Center (SCEC, Contribution 15047). SCEC is funded by NSF Cooperative Agreement EAR-2225216 and USGS Cooperative Agreement G24AC00072.

Abstract

Over geologic time, initiation and growth of upper crustal plate boundary faults, such as those that host current Earth's largest earthquakes, are influenced by thermally localized ductile shear zones (DSZs) in the lower crust. Today, DSZs influence elastic loading over the earthquake cycle, and the down dip extent of ~M≥6.8 earthquakes that rupture to the brittle ductile transition. The down dip rupture extent of large earthquake is poorly constrained by surface slip and seismic moment-rupture area relations.To begin to address rheological controls on DSZs we conduct 1D numerical calculations that couple ductile strength, shear heating and heat conduction. Spontaneous shear localization from thermal weakening arises at steady state within a fixed length region at a constant background temperature. The combination of a 1D geometry, fixed length and background temperature, and the assumption of steady state results in highly thermally constrained DSZs. The spatial strain rate distributions are approximately Gaussian allowing for a perturbation analysis. There is a characteristic width where strength is minimized and shear is localized at the lowest possible energy release rate. This scale is determined by a balance between the rheology's opposing temperature weakening and strain rate strengthening. DSZ width depends strongly on the choice of rheology. Contrasting with quartz (dislocation creep), rather than localizing, talc (glide) tends to deform via broadly distributed shear even at highly elevated loading rates. Distributed shear in talc is also expected at natural conditions; talc is too weak at natural loading rates to produce a thermal width smaller than the strike normal dimension of the largest natural occurrences.

Introduction

Recently, SCEC compiled and analyzed data that can be used to constrain deformation at and below the brittle ductile transition in southern California: the Southern California Earthquake Center Community Thermal and Rheology models (CTM, CRM) (Thatcher et al., 2016; Hearn et al., 2020; Hearn et al., 2026). These efforts were focused on establishing the ambient temperature at depth (CTM), and the lithology below the BDT (CRM). Doing so allowed the bulk rheology and therefore the bulk ductile strength to be determined below the BDT throughout this region. While these projects were successful (https://southern.scec.org/research/ctm; https://southern.scec.org/research/crm), they stopped short of addressing rheological properties that influence the down dip co-seismic rupture extent within San Andreas system. For instance, determining the rheology, degree of localization and expected width of DSZs underlying the faults in the region. Despite their mechanical importance to deformation in the brittle crust above and the hazard associated with down dip extension, relatively little is known about DSZ properties such as strain rate, strength, and width, because of difficulties in reliably estimating them from surface instrumentation. The stopping point of the SCEC CRM is the starting point for the present study, to better constrain the degree of localization of ductile shear zones beneath beneath plate boundary scale strike slip faults.

The more immediate and modest objectives of this study are to better understand the role of rheology in the thermal localization that determines the strain rate distribution and width of DSZs. Specifically, determining how the choice of rheology affects localization and, given a choice, the influence of particular environmental variables and rheological parameters.

Methodology

The 1D steady-state heat conduction equations for a distributed ductile heat source are:

$$\frac{d^2T}{dx^2} = -\frac{\tau}{k}\frac{dV}{dx} \quad (1)$$

and

$$\frac{d^2V}{dx^2} = \frac{\partial\dot{\gamma}}{\partial T}\frac{dT}{dx} \quad (2)$$

T is temperature, x is space, τ is shear stress, k is the thermal conductivity, V is velocity and $\dot{\gamma}$ is strain rate. The partial derivative in (2) is specified by the particular ductile flow law of interest. These equations were solved numerically in a fixed length 1/2 region, L/2 = 15 km. The region, boundary conditions and a schematic strain rate distribution are shown in **Figure 1**.

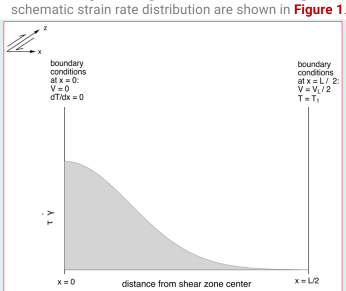

Figure 1: Schematic steady-state heat generation from shear heating with conduction in 1 spatial dimension, as appropriate for vertical strike slip. The associated boundary conditions are as labelled. V_L is the loading velocity (plate rate). In the calculations the background T_1 = 400°C, L=30 km, k= 2.5 Joules/m s °K while V_L is varied between the SAF plate rate of 1 nm/s up to 100 nm/s

Results

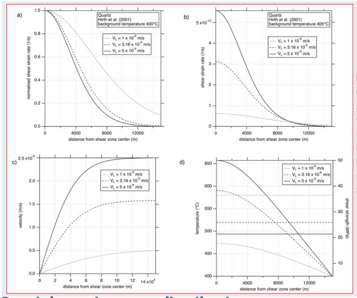

quartz
Hirth et al. (2001)

Figure 2: Calculations with quartz dislocation creep in a 15 km wide half region for 3 loading rates, V_L. a) Normalized strain rate. b) Strain rate /s. c) Velocity m/s. d) Temperature °C (left axis) and shear strength (right axis).

Spatial strain rate distribution.

In **Figure 2b** the $\dot{\gamma}$ distributions in x appears characteristic; it is approximately Gaussian (**Figure 3a**), allowing for a perturbation analysis of shear zone strength with width, l_c (**Figure 3b**)

$$\dot{\gamma}(x) = \dot{\gamma}_o exp\left[-\left(\frac{x}{l_c}\right)^2\right]$$

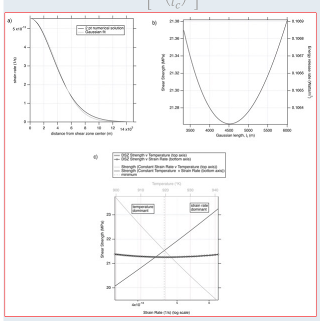

Figure 3: Perturbation of a Gaussian strain rate distribution. a) Fit of the strain rate distribution for quartz with L=30 km and VL=5 nm/s (black) to a Gaussian (grey). The numerical solution is the same as shown for the VL=5 case in **Figure 2**. b) The shear strength of a quartz Gaussian strain rate distribution as l_c is varied. c) Same shear strength data as in b) but plotted against average shear zone temperature (grey heavy line, top axis) and log average shear zone strain rate (black open circles, bottom axis, log scale). The vertical dashed line marks the minimum strength. Shown for reference are the temperature dependence of quartz strength at constant strain rate (grey, top axis) and strain rate dependence of strength at constant temperature (black, bottom axis).

Shear zone localization is control by the opposing temperature weakening and strain rate strengthening of the rheology. These balance when shear strength doesn't change with l_c, the minimum strength in **Figure 3b** and **3c**, or

$$\frac{\partial\tau}{\partial\dot{\gamma}}\frac{d\dot{\gamma}}{dl_c} = -\frac{\partial\tau}{\partial T}\frac{dT}{dl_c} \quad (3)$$

and characteristic width coincides with the minimum strength. Equivalently this is a minimum in the rate that energy (heat) is generated by shear, per unit area within the entire region.

Rheological controls.

As **Figure 3** implies, shear zone width is controlled by the rheological parameters (dependences on T and $\dot{\gamma}$). When the rheology is different (**Figure 4**), localization differs.

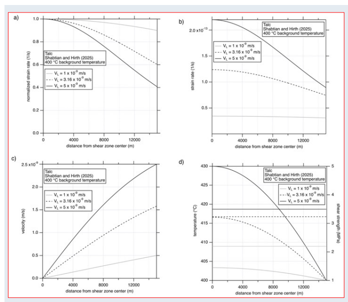

talc
Shabtian and Hirth (2025)

Figure 4: Calculations with talc dislocation glide and variable V_L in a 15 km wide half region, for comparison with quartz (**Figure 2**). a) Normalized strain rate. b) Strain rate /s. c) Velocity m/s. d) Temperature °C (left axis) and shear strength (right axis).

In contrast to quartz at the same loading rates, talc deformation is much more broadly distributed (**Figure 4a** and **b**). Quartz is self-localized at these loading rates and temperature weakening (**Figure 3d**), whereas talc is strain rate strengthening at the same rates (**Figure 4d**). These contrasts result from the significant rheological differences, shear strength in particular

Region & environmental controls

In addition to the rheology, there are controls from geometry and boundary conditions. The combination of 1D, fixed length and background temperature, and the assumption of steady state results in highly thermally constrained DSZs. Notably, when shear zones are thermally localized, they are self-similar, as seen when amplitude and length are normalized (**Figure 5**).

self-similar shear zones

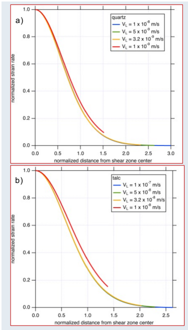

Figure 5: Self-similarity. a) Normalized quartz shear zones, V_L=1 to 10 nm/s. b) Normalized talc shear zones, V_L=10 to 100 nm/s. c) Normalized quartz (V_L=10 nm/s) & talc (V_L=100 nm/s) shear zones.

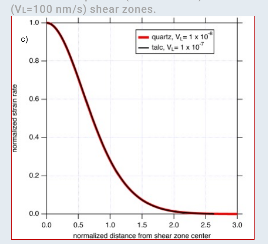

There are reasons to expect self-similarity in 2D steady-state (TBD), speculation at this point. Scaling of shear zone width and temperature are also highly constrained and rheology independent (**Figure 6**)

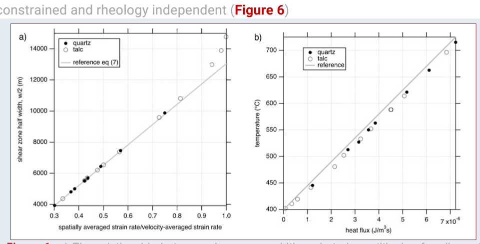

Figure 6: a) The relationship between shear zone width and strain partitioning for all quartz and talc simulations. Shown for reference is equation (4) in heavy grey. b) Relation between temperature change and heat flux for all quartz and talc simulations. The grey reference line is from equation (5), see text for discussion.

The reference line in **Figure 6a** is

$$w = \lambda L\frac{\hat{\dot{\gamma}}_s}{\hat{\dot{\gamma}}_v} \quad (4)$$

w = width, λ = degree of localization, L = regional length, $\hat{\dot{\gamma}}_s$ = spatially averaged strain rate, $\hat{\dot{\gamma}}_v$ = velocity averaged strain rate. For thermally localized shear, all of the RHS variables in (4) are constant except the spatially averaged strain rate, which is the ratio of loading rate to regional length. This is another indication that all the shear zones are self-similar except for talc at very low strain rates. These low strain rate talc shear zones (**Figure 4**) are not localized within the 30 km region. They are too weak to generate enough shear heat at these (natural) loading rates to self-localize. This is analogous to natural formations with narrow strike normal extent; these will always deform by broadly distributed shear. The largest strike normal extents of surface adjacent talc deposits have w < 80 m (Parseval et al., 2024; Zheng et al., 2026; Gondin and Jiang, 2004). Thus, natural talc is not of sufficient dimension to form DSZs at background temperatures this low.

The reference line in **Figure 6b** is the solution to equation (1) for a generic heat source symmetric about the region center,

$$T = T_1 + \frac{\tau\dot{\gamma}L^2}{8k}\left[1 - \left(\frac{2x}{L}\right)^2\right] \quad (5)$$

The similar dependence on spatial coordinate of all of the shearing calculations to (5) reflects the strong 1D steady-state regional constraint on the temperature distribution

References

Gondin, A.C., and S.Y. Jiang, (2004), Characteristics and genetic models for the talc deposits in Parana and Bahia, Brazil, Act Petrologica Sinica, 20, 829-836.

Hearn, E., M. Oskin, G. Hirth, L. Montesi, W. Thatcher, W. Behr, and E. Pauk (2020). The SCEC Community Rheology Model (CRM). Poster Presentation at 2020 SCEC Annual Meeting.

Hearn, E., Hirth, G., Oskin, M., Montesi, L., Behr, W., Legg, M., & Morelan, A. (2026). The SCEC Community rheology model for the southern California lithosphere: Geological framework, ductile flow laws, and preliminary implications. Earth and Space Science, 13, e2025EA004401

Hirth, G., C. Teyssier, and W. J. Dunlap, (2001), An evaluation of quartzite flow laws based on comparisons between experimentally and naturally deformed rocks, *Int. J. Earth Sci., 90*, 77-87.

Parseval, P.d., S.Y. Jiang, F. Fontan, R. Wang, F. Martin, and J. Freeet, (2004), Geology and ore genesis of the Trimouns talc-chlorite ore depost in Pyerenees, France, Acta Petologica, Sinica, 20, 877- 886.

Shabtian, H. S., & G, Hirth. (2025), Creep of talc at subduction zone conditions: Implications for slow slip and strength of the lithosphere, Geophysical Research Letters, 52, e2025GL116641.

Thatcher, W.R, Chapman, D.S., Williams, C,F., (2016)Building a Community Thermal Model for Southern California Using Heat Flow, Geologic, Seismologic and Petrologic Constraints II: Model Formulation and Bounds on Geotherms, American Geophysical Union, Fall Meeting 2016, abstract #T13A-2684

Zheng, J., G. Hu, H. Chen, X. Li, H. Wu, X. Li, N. Ding, W. Sun, J. Zhao, P. Li and F. Chang (2026), Genesis of magnesite-talc-brucite deposits in Paleoproterozoic Mg-rich carbonate formations, Liaogong Peninsula, northeast China, Ore Geology Reviews, 192.